Engineering Failure Analysis 117 (2020) 104813

Contents lists available at ScienceDirect

Engineering Failure Analysis

journal homepage: www.elsevier.com/locate/engfailanal

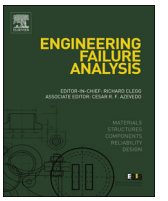

Remote inspection of RC structures using unmanned aerial vehicles and heuristic image processing

D. Ribeiro[a,*], R. Santos[a], A. Shibasaki[b], P. Montenegro[c], H. Carvalho[d], R. Calçada[c]

[a] CONSTRUCT, School of Engineering of Polytechnic of Porto, Portugal
[b] School of Engineering of Mackenzie Presbyterian University, Brazil
[c] CONSTRUCT, Faculty of Engineering of University of Porto, Portugal
[d] Minas Gerais Federal University, Brazil

ARTICLE INFO

Keywords:
Remote structural inspection
UAV
Digital image processing
Heuristic feature-extraction
BIM

ABSTRACT

This article describes an innovative methodology for remote inspection of reinforced concrete (RC) structures using Unmanned Aerial Vehicles (UAVs) and based on advanced digital image processing. The use of specific heuristic feature-extraction methods, developed in MATLAB©, allows the automatic identification of various types of RC pathologies, particularly, biological colonies, efflorescences, cracks and exposed steel rebars. The developed inspection methodology is applied to the Monte da Virgem telecommunications tower, which has a total height of 177 m and is the highest structure of this kind in Portugal. The results demonstrate the efficiency and robustness of the methodology in: i) its ability to accurately locate and characterize the existing pathologies, ii) visualizing the full extent of pathologies in 3D photogrammetric reconstitutions of the structure, and iii) integrating the identified pathologies into a Building Information Modeling (BIM) model. The regular use of the proposed methodology over time will allow accurate monitoring of the evolution of pathologies to assess the condition of the structure. Additionally, the integration of the inspection results into BIM digital models will help infrastructure managers to decide on the implementation of the most adequate facility management strategies in order to optimize the scheduling of maintenance, rehabilitation and retrofitting interventions.

1. Introduction

General assessment of civil engineering assets is a key instrument for infrastructure managers to evaluate structural integrity and operability, and estimate possible maintenance or rehabilitation needs. Typically, the assessment of conditions is performed based on information obtained by visual inspections [1] and/or Structural Health Monitoring (SHM) systems [2].

Visual inspections require the presence of trained inspectors who directly assess the structural condition based on specific decision-making criteria. This traditional technique is generally time-consuming, laborious, expensive and may put the safety of professionals at risk, particularly in situations with difficult accessibility.

In turn, SHM systems allow the continuous monitoring of structural integrity based on the measurement of physical quantities, such as accelerations, strains and displacements, in order to enhance safety and reliability, and reduce inspection costs. However, these systems typically have limited spatial coverage or require dense instrumentations arrays. Moreover, once installed, access to the

* Corresponding author.
E-mail address: drr@isep.ipp.pt (D. Ribeiro).

https://doi.org/10.1016/j.engfailanal.2020.104813
Received 30 March 2020; Received in revised form 29 July 2020; Accepted 10 August 2020
Available online 12 August 2020
1350-6307/

sensors is often restrained, making regular system maintenance difficult, as well as the eventual detection of sensory system malfunctions and noisy signals.

To address some of these problems, digital images and their associated processing techniques have been recognized as key components for improving inspection and monitoring strategies in order to achieve an automated assessment of the conditions of civil engineering infrastructures [3]. For condition assessment purposes, the methodologies based on digital images generally consist of: a) image collection, b) image processing and analysis, and c) integration of the results with other technologies/platforms.

The most recent lines of research are mainly focused on image processing and analysis, particularly in the development of automated damage identification techniques, including concrete cracks [4], concrete spalling and delamination [5], efflorescences [6], fatigue cracks [7] and steel corrosion [8]. Some of the reported pathologies are not related to concrete degradation. Nevertheless, the applied techniques have the potential to be adapted to RC structures. In any case, the existing bibliography is still very scarce on topics such as biological colonies and exposed steel rebars.

In this domain, two main approaches for damage identification based on digital images are presented in the bibliography: heuristic feature-extraction methods [9,10] and deep learning-based methods [11,12].

The heuristic feature-extraction methods rely on the application of filters [9,13], or machine learning classifiers [14] to images in order to enhance features of interest.

Much of the early research on vision-based damage detection was focused on the identification of concrete cracks based on heuristic filters, particularly edge detection filters, e.g., Sobel gradient filters and the application of the Canny method. These filters are able to detect boundaries between areas of the image with different brightness and reveal particular textures, enabling the location of the pixels on the crack edges [15]. Li & Zhao [16], Wang et al. [17] and Kim et al. [18] pointed out that the efficiency of heuristic edge detection filters in the identification of concrete cracks is negatively influenced by perturbations on concrete surfaces, such as roughness, stains and pockmarks, and by induced external noises, such as light conditions, distortions, shadows or blur. Cha et al. [4] studied the use of denoising techniques to reduce noise from image data and enhance image edge detection.

Another type of heuristic features are the morphological filters related to image processing operators based on shape modifications [19]. In a morphological operation, the value of each pixel in the transformed image is based on a comparison of the corresponding pixel in the original image with its neighbors. The most basic morphological filters are dilation and erosion. Dilation adds pixels to the boundaries of objects in an image, while erosion removes pixels from the boundaries of objects. Some variants of these morphological filters are also used, such as, opening, closing and binarization operations [20]. Image binarization, which allows converting pixels from a grayscale image to either black or white, is commonly used for crack detection, because dark cracks are generally categorized as black, whereas lighter regions of the image appear white [18].

Nishikawa et al. [21], Mohan & Poobal [22] and others, proposed crack detection strategies based on multiple sequential image filtering, because the use of a single heuristic feature is usually not sufficient for reliable crack detection. In the detection of steel corrosion, researchers typically use strategies based on spectral filters, related to the distinct reflectivity between steel and concrete, in conjunction with color filters, taking advantage of the color contrast between corroded steel and concrete [8].

Barkavi & Natarajan [9], Oyekola et al. [23], Xu et al. [11] and Kim & Cho [24], refer that heuristic features, based on edge detection algorithms and morphological features, have limitations, namely, the inability of the algorithms to cover all the distinct and unexpected situations of real-world applications, the fact that they rely heavily on manual parameters, and also because they typically require the prior removal of external environmental perturbations from the images due to its limited performance on noisy image data. To overcome some of these limitations, more recently, heuristic features based on machine learning classifiers were successfully developed, particularly, Wavelet transforms, Principal Components Analysis, randomized Hough transforms and Otsu's method [22,25].

Alternatively, deep learning computer vision methods have been successfully applied in the last few years in vision-based damage detection of civil engineering infrastructures. A number of deep learning algorithms are broadly used in computer vision specifically for features learning and classification of images [3,26]; however, the most widely and successfully applied are Convolutional Neural Networks (CNNs) [11,27]. CNNs were specifically designed for crack identification and involve a training procedure based on a large set of real-world images, representative of crack and non-crack scenarios, and the definition of a classification model based on a group of successive layers (convolution, pooling and fully-connected layers) associated to specific mathematical operators [4]. The trained classification model is subsequently applied to new images in which cracks are to be detected. However, Ciresan et al. [28] pointed out that CNNs have demanding hardware requirements and can be extremely time-consuming, especially during the training and validation phases, even if advanced GPU processing is available.

More recently, Rakha & Gorodestsky [29], Kim et al. [30], Kim et al. [31] and Omar & Nehdi [32] presented some applications regarding the use of Unmanned Aerial Vehicles (UAVs) coupled with computer vision systems for remote structural inspections. These coupled systems have proven to be competitive in identifying damage in inaccessible and extensive areas, allowing a considerable reduction of costs and execution times, since the inspection requires less technical staff. However, the performance of digital image processing tools depends highly on the image acquisition conditions, such as capturing angle, light quality, weather conditions and undesired dust in the air or on the surface of the target. Dung et al. [7] performed the monitoring of an entire steel bridge using UAVs for damage identification. The authors pointed out that images taken from UAVs (and in particular from UAVs of the multicopter type) are bound to present some degree of loss of sharpness and focus due to the fact that they are taken from moving and unstable platforms. Therefore, more robust and efficient image classifiers should be adopted, because the above conditions are not usually considered in CNNs training. Dorafshan et al. [33] refer some challenges concerning the use of UAVs in bridge inspections that are not met by actual commercial UAVs, particularly: the importance of using small-sized models, having more reliable positioning systems instead of the classical GPS signals, upgrade in wind and turbulence endurance, 360° gimbals, adjustable light source onboard,

camera exposure control and optical zoom. Silva & Lucena [26] refer that UAVs enable the collection of larger image datasets, at least a few orders of magnitude higher, compared to the traditional visual inspections using cameras. The authors emphasize the importance of extracting meaningful features from such an extensive amount of data so that more time can be dedicated to data analysis.

Thus, this study aims to make clear and effective contributions regarding some aspects that are presently not sufficiently addressed in the existing bibliography, particularly:

- Concerning the image collection, the proposed methodology is based on photographic cameras incorporated in UAVs, thus enabling structural inspection even in cases with limited accessibility. Flights may be preprogramed or manually controlled and the images collected are georeferenced, enabling the exact location of pathologies and the precise monitoring of their evolution based on specific damage indicators. Furthermore, the results of the inspection are presented by means of 3D geometric reconstitutions obtained through photogrammetry based on point-clouds.
- In relation to the image processing and analysis, the proposed methodology is based on heuristic image processing. Compared to other methodologies reported in the bibliography concerning mostly the detection of cracks, the proposed methodology has a wider range of application, since it also allows the detection of efflorescences, biological colonies and exposed steel rebars.
- The integration of inspection results into BIM digital models is also an added value to the proposed methodology that will allow infrastructure managers to closely monitor the evolution of pathologies. In particular, BIM models contribute to facility management, helping to prioritize the areas that need intervention or to plan the intervention of maintenance teams, among others.

After the introduction, section 2 presents an overview of the proposed methodology for remote inspection of RC structures based on advanced image processing and UAVs. Section 3 presents a detailed description of the computational tools developed for the automatic identification of pathologies. Afterwards, section 4 describes the application of the proposed methodology to the inspection of the Monte da Virgem telecommunications tower, including the BIM integration. Finally, in section 5, the main conclusions drawn from the present work are listed along with the major achievements.

2. Methodology for the remote inspection of structures using UAVs

Fig. 1 schematically presents the proposal of a methodology for the inspection of structures using Unmanned Aerial Vehicles (UAVs), also known as drones, based on automated digital image processing, and their subsequent integration into Building Information Modeling (BIM) models.

Phase 1, recognition and preparation, typically involves: i) the collection of project elements and the investigation of the inspection history of the target structure, ii) a site-visit to assess conditions and possible risk factors (potential flight obstacles, wind exposure conditions, electromagnetic interference, etc.), iii) obtaining flight permits from the competent national authorities, iv) selection of the technical staff and flight equipment (drone, camera, etc.), v) elaboration of a flight plan including the definition of landing/takeoff zones, the flight time, the strategy for collecting images of the structure, the proximity of the drone to the target, among others.

Phase 2, collecting images with UAV, involves, in the first stage, a precision topographic survey of some control points of the structure. This step is essential for the georeferencing and calibration of the collected images and their subsequent incorporation into the BIM model. Control points must be located along the entire structure and can be materialized with auxiliary targets, or, alternatively, with remarkable points of the structure. Obtaining the coordinates of the control points involves the definition of ground basepoints, in polygonal, and in line-of-sight with the structure, with the support of GNSS (Global Navigation Satellite System) receivers, preferably with the support of a RTK (Real Time Kinematics) module, in addition to the use of an electronic theodolite.

In the second stage of phase 2, images are captured using a drone equipped with a photographic camera. The drone must meet a set of specifications, namely: wide range of control and operability, endurance to wind loads in the vehicle and camera, stabilization capability, must include obstacle proximity sensors, positioning accuracy via RTK system, possibility of automatic flight,

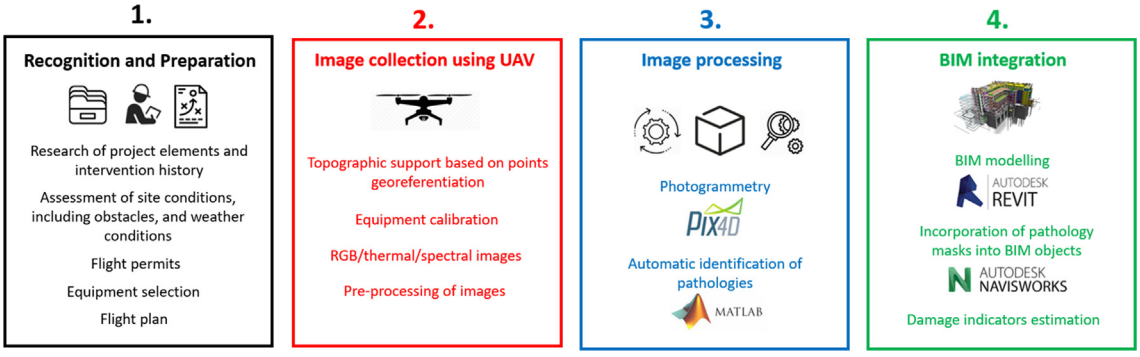

Fig. 1. Methodology for remote inspection of structures using UAVs.

compatibility with different type of cameras or equipment, high autonomy, high-resolution cameras and high storage capacity. The collection of images must be done safely, but as close to the structure as possible, since shorter distances improve image resolution.

Phase 3, image processing and analysis, involves two stages: i) the reconstruction of a 3D geometric model of the structure based on georeferenced images and applying photogrammetry techniques available in the Pix4Dmapper software, and ii) the automatic identification of pathologies based on the collected images and through the application of image processing tools available in the Image Processing Toolbox of the MATLAB© software [34].

Regarding the 3D geometric model of the structure, Pix4Dmapper uses an algorithm that accesses the properties of each image (camera specifications, georeferencing, resolution, etc.) saved on the associated EXIF (EXchangeable Image File) to create a virtual point-cloud model, using common points across the images. The point-cloud model captures, in many situations, neighboring objects or background noise (trees, sky, buildings, etc.) that appear in the images and must be removed. Regarding the digital image processing phase, the available tools were directed to the identification of typical pathologies in RC structures, namely biological colonization, cracks, exposed steel rebars and efflorescences. The computational tools developed in MATLAB© for each of the pathologies are described in Section 3. Processed images resulting from the application of these computational tools, in which the pathologies are marked, are then overlaid on top of the original images, using an overlay operation available in the MATLAB© software.

Phase 4, consists in integrating the image with the identified pathologies into the BIM model, and involves two stages: i) the incorporation of the mask associated with a certain pathology into the BIM model developed in the Autodesk Revit platform, and ii) the quantification of damage indicators based on measurements taken directly from the images. The image with marked pathologies is superimposed on the BIM model using the Autodesk Navisworks software. The damage indicators are estimated in MATLAB© and are typically related to the total length of the crack, the total area of biological colonization or efflorescences, among others.

3. Tools for the automatic identification of pathologies

The automatic identification of pathologies was performed using the MATLAB© Image Processing Toolbox based on heuristic feature-extraction methods. Depending on the type of pathology, edge detection features were used in conjunction with morphological features. The main implementation aspects of the tools developed for the identification of biological colonies, efflorescences, cracks and exposed steel rebars, all in RC structures, are presented in the following subsections. The MATLAB© commands used in the algorithms will be denoted in italics in the text below and indicated within the figures.

3.1. Biological colonies and efflorescences

The tool for detecting biological colonies and efflorescences is based on image segmentation. Image segmentation is based on the division of an image into regions according to a criterion that distinguishes groups of pixels (e.g. color segmentation). In these circumstances, the usual color of each pathology is what differentiates it from the others, so yellow was used for the biological colonies and white was used for the efflorescences. Fig. 2 shows the ordered sequence of the morphological features that constitute the identification algorithms, including a graphical representation of the effect of the application of the features for both pathologies.

First, from the original image, an adjustment is made on the image contrast, applying the *histeq* command, in order to guarantee the equalization of the image's color histogram (R - red, G - green and B - blue).

Then, segmentation features were applied to both original and contrasted images, using the *color thresholder* application. The segmentation feature for the identification of biological colonies involved the elimination of band B from the image, since the junction of bands R and G results in yellow. The segmentation feature for the identification of efflorescences resulted from a trial and error adjustment of the levels of R, G and B bands, resulting in optimal values for each of the bands in the range between 200 and 255. The dual application of the segmentation features, both to the original and contrasted images, and the subsequent addition of the resulting images, improved the robustness of the algorithm regarding its ability to identify all yellow and white pixels, since the contrast adjustment on the original image may be insufficient to distinguish yellow from white. Segmentation features result in a binary image in black and white. Finally, the pathology is shown superimposed on the original image using a false color by means of the *imoverlay* MATLAB© command.

The extent of the pathology is estimated based on the information of the binary image, which, in practice, consists of a 2D array with zero values for the black pixels, and unit values for the white pixels, which correspond to the pathologies.

Thus, the total area of the pathology (A) is estimated by multiplying the number of white pixels (n_w), obtained through the *sum* command, per the pixel area, which is equal to the squared pixel dimension (d_{px}):

$$A = n_W . d_{px_i}^2 \tag{1}$$

The pixel dimension is obtained through the optics principle, illustrated in Fig. 3, regardless of the horizontal and vertical directions [35]:

$$d_{px} = \frac{D}{f} . \frac{h}{n_{px,h}} = \frac{D}{f} . \frac{v}{n_{px,v}} \tag{2}$$

where f is the focal distance of the camera, h and v are the horizontal and vertical dimensions of the camera sensor, D is the distance between the camera sensor and the target, H ($= d_{px} \times n_{px,h}$) is the horizontal dimension of the field of vision, V ($= d_{px} \times n_{px,v}$) is the

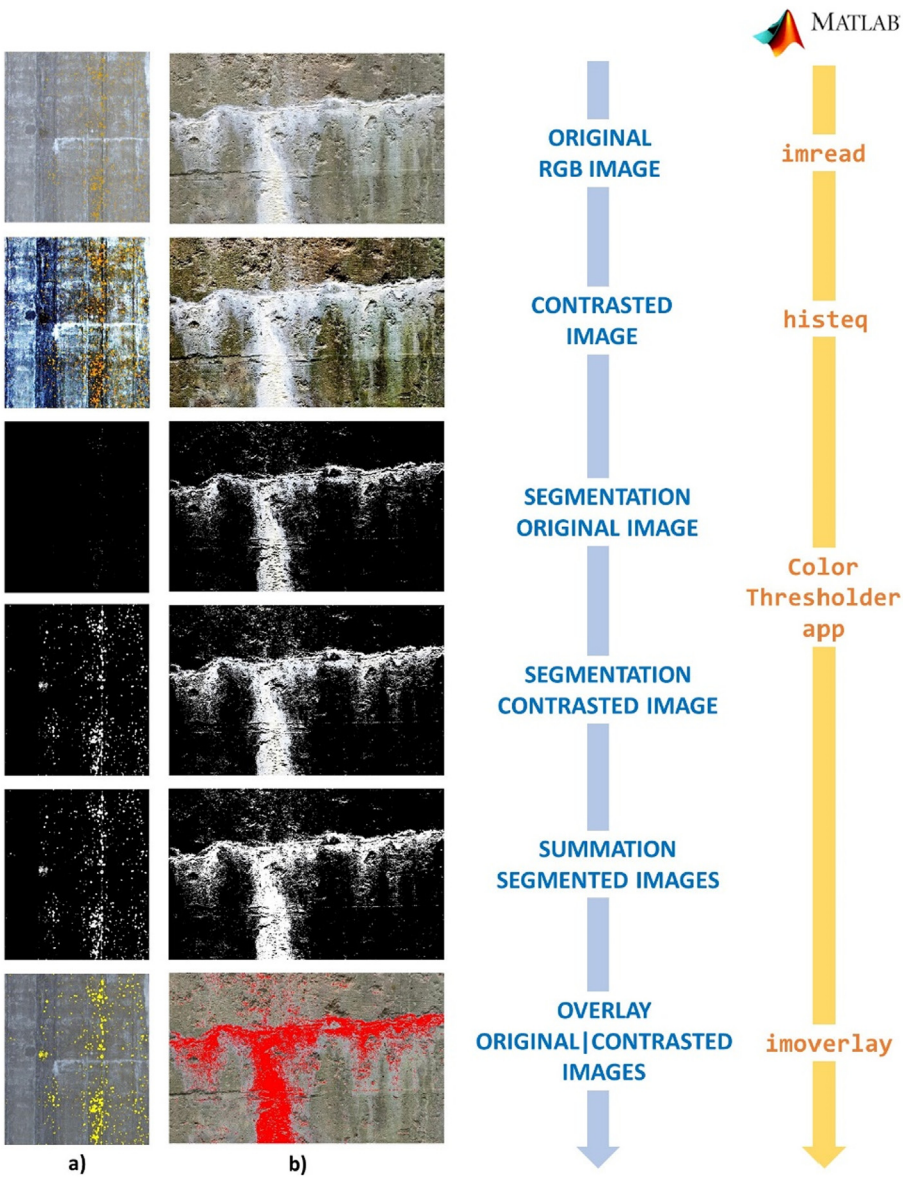

Fig. 2. Methodology for identifying: a) biological colonies, b) efflorescences.

vertical dimension of the field of vision, $n_{px,h}$ and $n_{px,v}$ are the number of pixels of the camera sensor in the horizontal and vertical directions. Parameters f, h, v, $n_{px,h}$ and $n_{px,v}$ are typically provided by the camera manufacturer. The distance D, between the video camera sensor and the target, is estimated based on a laser sensor installed in the UAV, which allows scaling the image. Lens distortions and perspective effects are both neglected.

3.2. Cracking

Processing crack images involves, firstly, the detection of the edges, and then, the application of morphological features that enhance their visualization and tracing precision (Fig. 4).

Edge detection involves the prior application of a gradient detection filter, which is able to identify areas of the image with abrupt changes in lightness, based on the gray scale image. The variation in the saturation is evaluated by calculating local derivatives of the image function, a discrete function with values ranging from 0 to 255 in correspondence with the image pixels, and with the help of matrix operators. This operation is performed by applying the Prewitt method [13], using the *imgradient* command. Afterwards, the automatic edge detection is performed by applying the Canny method [13], using the *edge* command, which is able to identify objects in the image by associating them in different clusters, which, in this particular analysis, are the clusters associated with cracks and the rest of the image. Edge detection requires the prior definition of the gray scale threshold value that distinguishes the tones of dark and

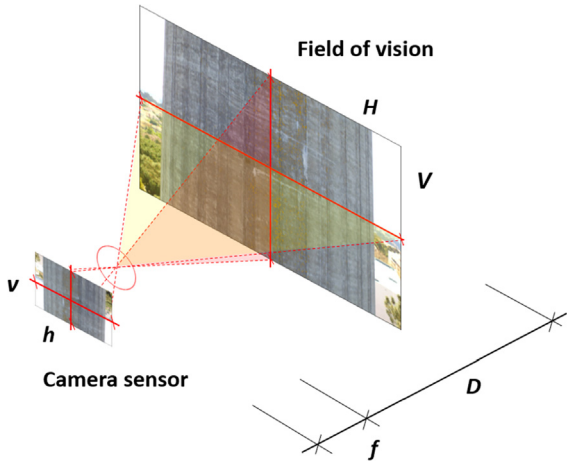

Fig. 3. Estimating the dimension of the pixel based on the optics principle of focal distance and field of vision.

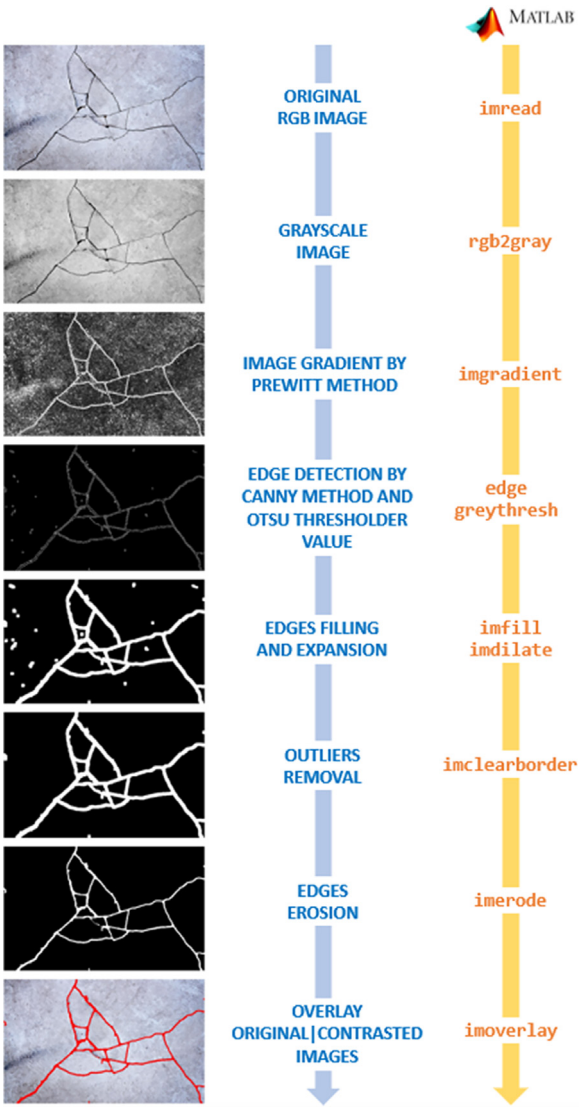

Fig. 4. Methodology for identifying cracks.

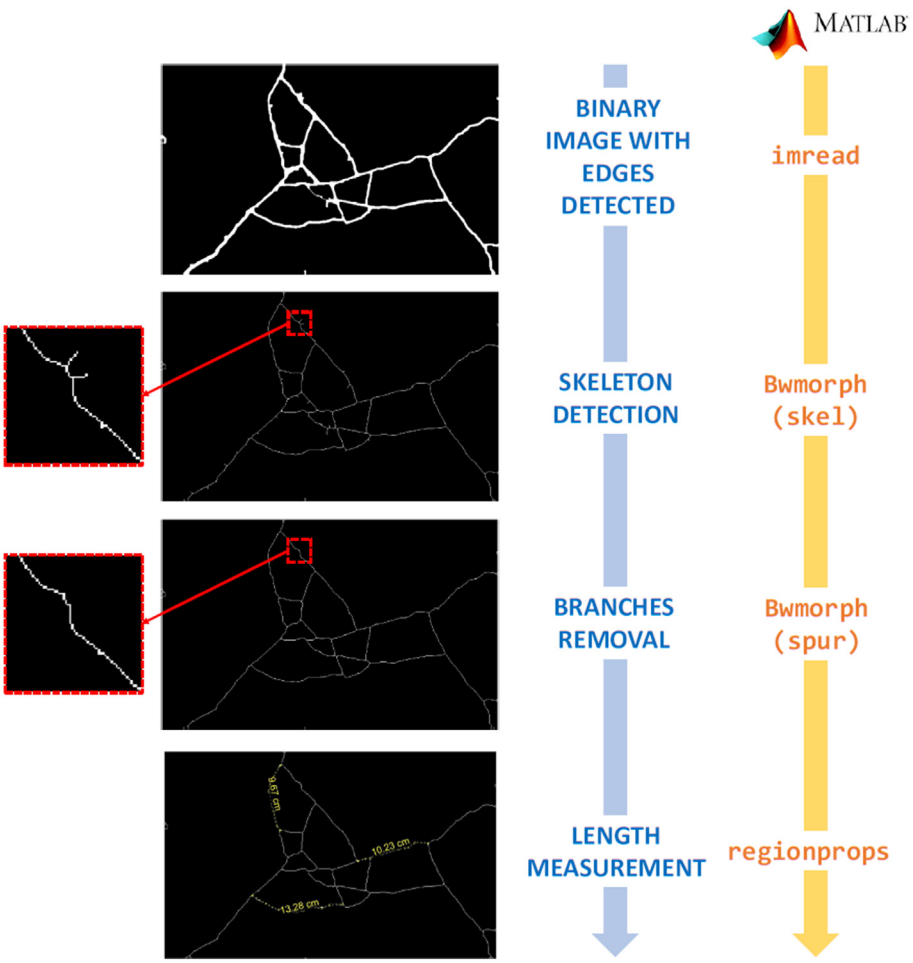

Fig. 5. Algorithm for estimating the crack length.

light gray. This threshold is automatically defined by the *greythresh* command, which is able to calculate the thresholder value using the Otsu's algorithm [13].

After detecting the crack edges, specific morphological features are applied, in particular: a) the closure (*imfill* command) that allows the filling of the crack area, b) the expansion (*imdilate* command) that allows the expansion of crack areas in the perspective of aggregation with nearby areas also identified as cracks, c) the elimination of outliers (*imclearborder* command) to remove objects outside the patterns of the cracks, d) the erosion (*imerode* command) that contracts the crack zones and defines the final contours, and finally, e) the pathology is shown in the image by means of a false color, resulting from the change in the white color of the binary image, and the superimposition on the original image using the *imoverlay* command.

The crack length is estimated based on the information of the binary image, which, in practice, consists of a 2D array with zero values for the black pixels, and unit values for the white pixels, which correspond to the pathologies.

First, the skeleton of the crack edges is performed, i.e., the definition of the crack axis, based on the *bwmorph* command through the *skel* operation. Afterwards, from the resulting image, a branch cleaning is performed, reusing the *bwmorph* command with the *spur* operation, in order to remove small and barely visible lines from the base skeleton, probably associated with false-positive occurrences. Finally, the total length of the crack can be estimated with a specific distance tool using the *regionprops* command. The algorithm for estimating the crack length is presented in Fig. 5.

The real dimensions of the image, in the horizontal (H) and vertical (V) directions, are required and estimated according to Fig. 3 and by applying Eq. (1). For scaling purposes, the distance between the video camera sensor and the target is estimated based on a laser sensor installed in the UAV. Lens distortions and perspective effects are both neglected.

3.3. Exposed steel rebars

The detection of exposed steel rebars, in many situations accompanied by visible corrosion phenomena, involved, first, adjusting the brightness of the original image, through the *imgshow* command and defining the brightness variation (typically between + 50 and + 100), so that only darker colors are visible. Then, the image was segmented by bands of colors (or channels), using the *imsplit*

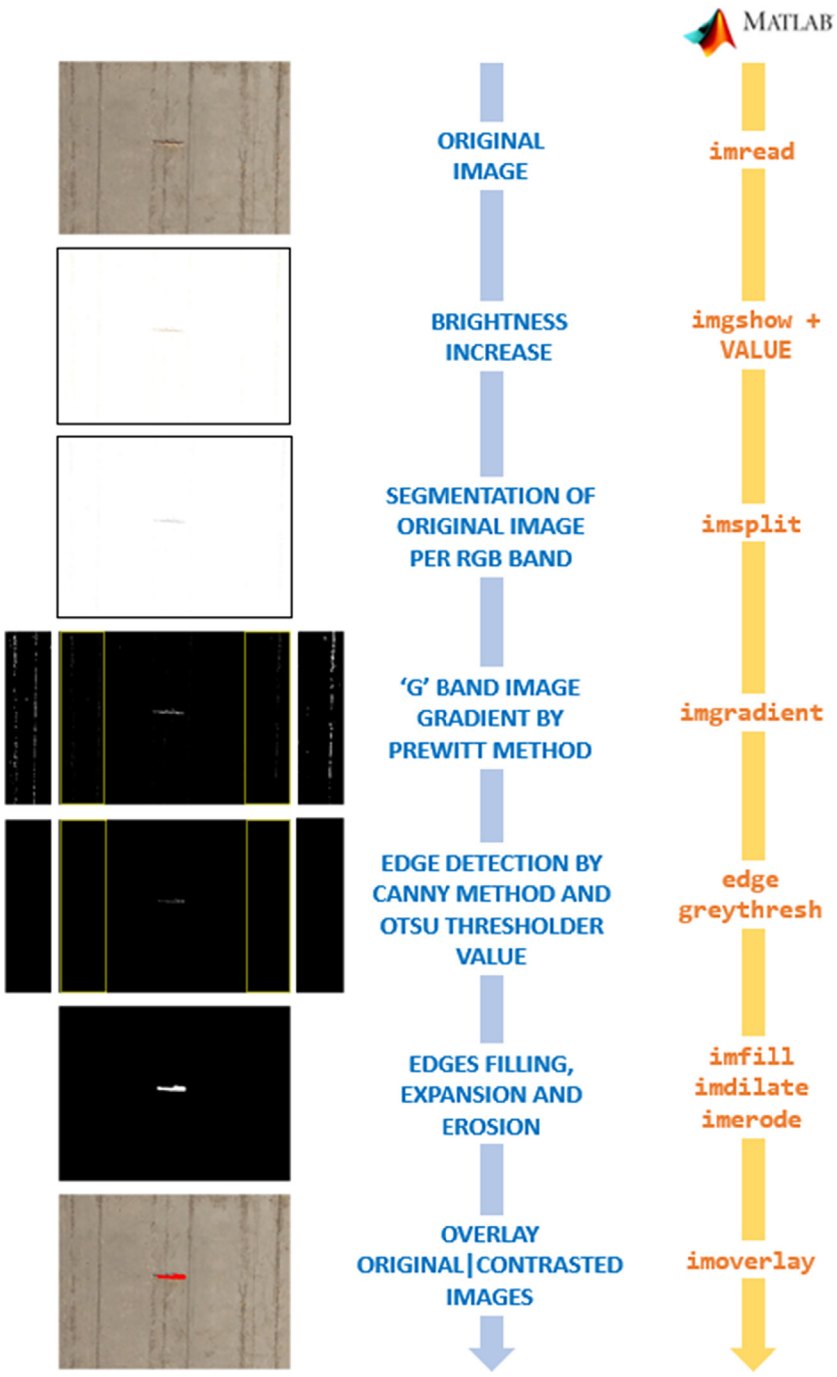

Fig. 6. Methodology for identifying exposed steel rebars.

command, and retaining only the G band, in which the darkest colors of the image were concentrated. Based on this image, a color gradient detection filter was applied, followed by edge detection, in a procedure identical to that applied in the identification of cracks but, in this case, with the purpose of detecting the edges of exposed steel rebars. Then, the morphological features of image filling, dilation and erosion were applied consecutively. Lastly, the pathology is shown in the image by means of a false color, resulting from the change in the white color of the binary image, and superimposed on the original image. Fig. 6 shows the sequence of features that constitute the identification algorithm, including a graphical representation of its application. Regarding gradient detection and edge detection filter operators, detailed views of the lateral parts of the images are also presented, including a digital adjustment of its brightness, in order to have a clearer perception of the differences between the results of both operators.

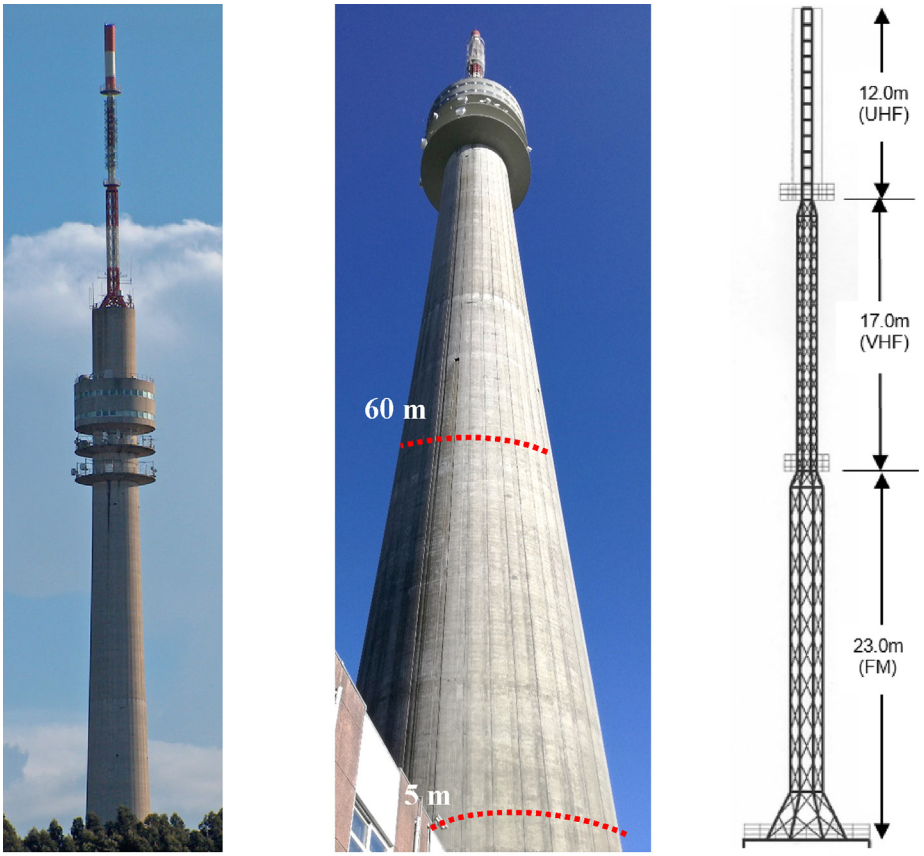

Fig. 7. Monte da Virgem telecommunications tower: a) general view, b) RC shaft, c) metallic mast.

4. Remote inspection of the Monte da Virgem telecommunications tower

4.1. Structural description

The Monte da Virgem telecommunications tower is a transmission tower built by Altice/Portugal Telecom in 1995 and located in Vila Nova de Gaia, in the north of Portugal. The structure of the tower consists of a 126 m high RC shaft and a 51 m high metallic mast, for a total height of 177 m. It is the highest structure of its kind in Portugal (Fig. 7a).

The RC shaft has the shape of a hyperboloid of revolution, with a circular hollow section and a diameter varying between 14.3 m, at the base, and 7.7 m at the top (Fig. 7b). The shaft includes five technical floors, materialized by prestressed concrete cantilever slabs. The technical floors are located between the heights of 94.9 m and 112 m, in relation to the base of the shaft, two of which are closed with external walls, while the three remaining floors are open with balcony railings.

The metallic mast consists of a spatial lattice composed of three sections along its height (Fig. 7c). The bottom section supports the FM transmission system, is 23 m high and has a maximum transverse dimension of 2.20 m. The middle section supports the VHF transmission system, is 17 m high and has a maximum transverse dimension of 1.20 m. The third and top section receives the UHF transmission system, is 12 m high and has a 0.64 m square cross-section, and is surrounded by a cylindrical polyester sleeve. The mast has an octagonal shape base fixed to a transition slab located at the top of the concrete shaft by means of anchor bolts. Additional details about the structure can be found in Ribeiro et al. [36].

4.2. Recognition and preparation

The inspection of the tower focused on the external part of the RC shaft, between the heights of 5 m and 60 m, in relation to the base of the structure (Fig. 7b).

The Monte da Virgem tower is located in Area 3 of the air Control Traffic Region (CTR) of Porto, Portugal. The rules for the use of UAVs in this area allow flights without formal authorization for operating heights below 80 m above the ground surface or up to the maximum height of the existing natural/artificial obstacles, considering a radius of 75 m centered on the aircraft.

The flight technique that was used was manual flight due to the following constraints: i) possible signal interference from the

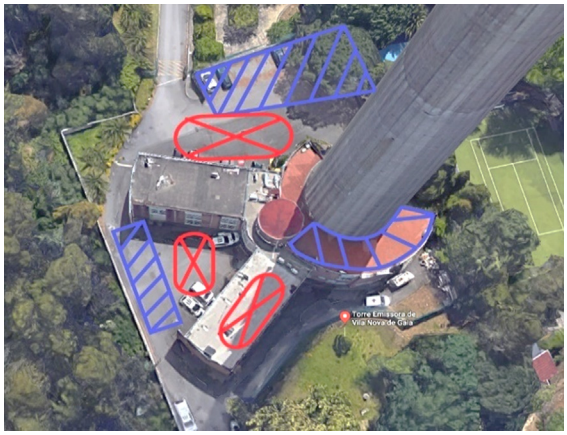

Fig. 8. Flight plan: observation zones (in blue) and take-off/landing zones (in red).

transmitting equipment operating in the tower, ii) the existence of trees near the base of the tower, iii) the complex geometry of the tower's surface, in the form of a hyperboloid of revolution, hindering the programming of automatic flights, and iv) due to the proximity of the coastline, the wind and the possible attack of birds, mainly seagulls, posed a threat to flight safety.

The strategy for collecting the images consisted in a photographic scan of the external concrete surface in an upward movement (from bottom to top), an adjustment with a lateral movement, followed by a downward movement (from top to bottom). These movements are repeated successively until the photographic survey of the entire perimeter of the shaft between the pre-established levels is complete.

In the flight plan, and according to the representation of Fig. 8, observation zones for the collection of images were defined, marked in blue, as well as take-off/landing zones, marked in red.

4.3. UAV image collection

The image collection was performed with a professional drone, namely a DJI Matrice 600 Pro (Fig. 9a). The DJI Matrice 600 Pro is a hexacopter weighing between 9.5 kg and 10 kg, with a maximum recommended take-off weight of 15.5 kg, a maximum horizontal speed of 65 km/h, a maximum service ceiling of 2500 m above sea level and an estimated flight autonomy of approximately 30 min (per battery set). The camera installed in the drone was a gimbal mounted DJI Zenmuse X5, with a MFT 15 mm focal length f/1.7 aspherical lens, a 16MPx resolution and a sensor with an imaging area of 17.3 mm × 13.0 mm (21.6 mm diagonal). The gimbal used ensures image stabilization along the three axes. The visualization of the images and the remote control of the drone were carried out by means of a DJI Matrice 600 Series remote controller and a high-resolution tactile DJI Crystal Sky monitor, with internal image storage capacity.

The topographic survey of the control points located in the shaft of the tower was performed using a Leica TRCP 1200 total station (Fig. 9b). The support points, four in total, were polygonally arranged with direct visibility to the tower shaft. Their coordinates were evaluated using a STNSEX S10 GNSS receiver, in RTK mode, with the corrections provided by the National Network of Permanent Stations (ReNEP).

The images were collected manually with the camera positioned obliquely in relation to the structure, at intervals of about 1.0 m in height, considering a minimum overlap of about 60%. The distance from the drone to the tower shaft varied between 5 m and 10 m. In total, about 6350 photographs were collected.

4.4. Image processing

The captured images were processed using the Pix4Dmapper software in order to reconstruct the 3D geometric model of the structure between the 5 m and 60 m levels (Fig. 10).

The automatic identification of pathologies based on the captured images and the application of the MATLAB© Image Processing Toolbox (according to the details of Section 3) is illustrated in Fig. 11 for the case of biological colonies (Fig. 11a), exposed steel rebars (Fig. 11b), efflorescences (Fig. 11c) and cracking (Fig. 11d). For each pathology, the original and transformed images are presented in parallel for comparison purposes. Biological colonies associated with the presence of lichens and mosses were identified mainly in the area of the shaft facing East, with less sun exposure. Exposed steel rebars were detected in specific cases and generally associated with corrosion phenomena, and efflorescences were identified in concrete joints and in areas where the concrete is more porous and permeable. No visible cracks were reported during the remote inspection and no false positive occurrences were identified.

Fig. 12 shows the automatic identification of biological colonies (Fig. 12b), efflorescences (Fig. 12c) and their coupling effect (Fig. 12d), using false colors and based on a portion of the concrete shaft of the Monte da Virgem tower (identified in Fig. 11a).

Fig. 9. UAV image collection: a) DJI Matrice 600 Pro in operation, b) topographic survey.

Fig. 10. Global perspective of the 3D geometric model of the structure reconstituted in Pix4Dmapper software.

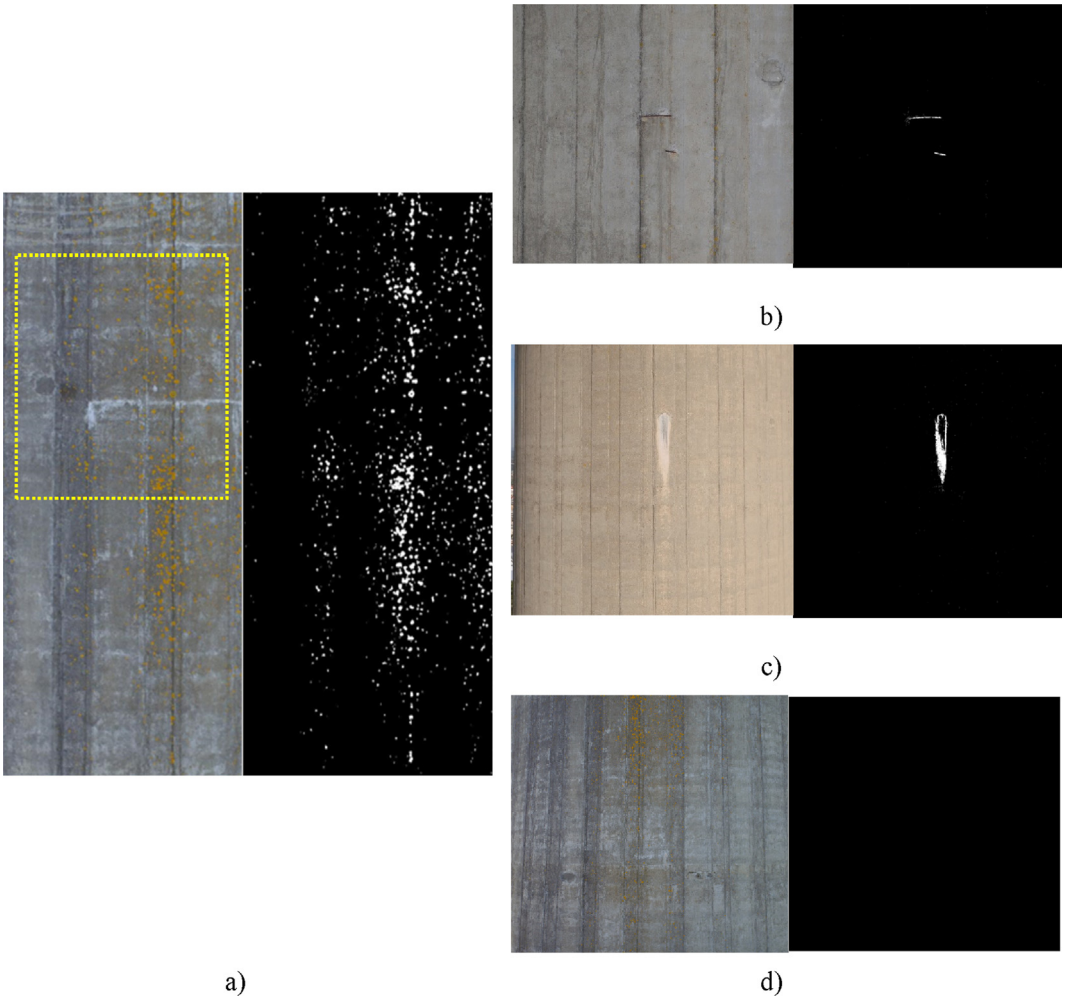

Fig. 11. Automatic identification of pathologies using the MATLAB© Image Processing Toolbox (after segmentation or edge detection and enhancement): a) biological colonies, b) exposed steel rebars, c) efflorescences, d) cracking.

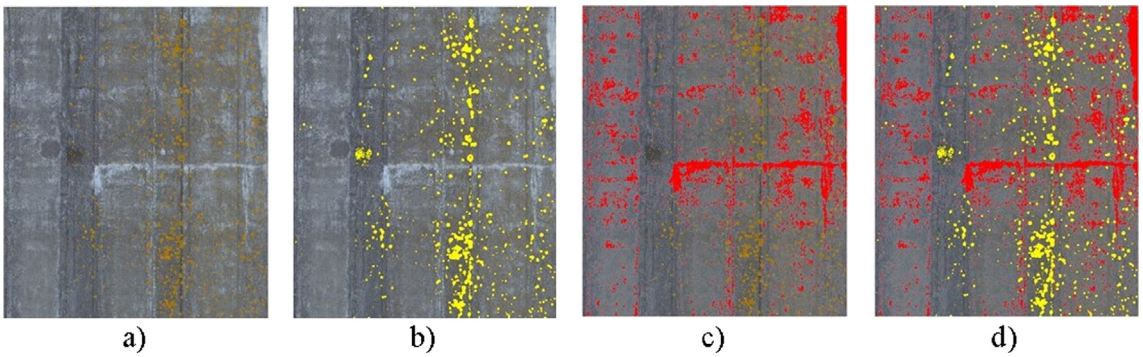

Fig. 12. Coupling effect between biological colonies and efflorescences (using false colors): a) original image, b) biological colonies (yellow color), c) efflorescences (red color), d) coupling effect.

Despite the similitudes between the routines for the identification of biological colonies and efflorescences (Section 3.1), the methodology demonstrated efficiency and robustness in the correct detection and separation of these two pathologies.

Fig. 13 illustrates the overlay of the images from the 3D geometrical model of the tower with the images from the MATLAB© Image Processing toolbox for identifying biological colonies (Fig. 13a), exposed steel rebars (Fig. 13b) and efflorescences (Fig. 13c). In all cases, the pathologies were represented using a false color, in this case red.

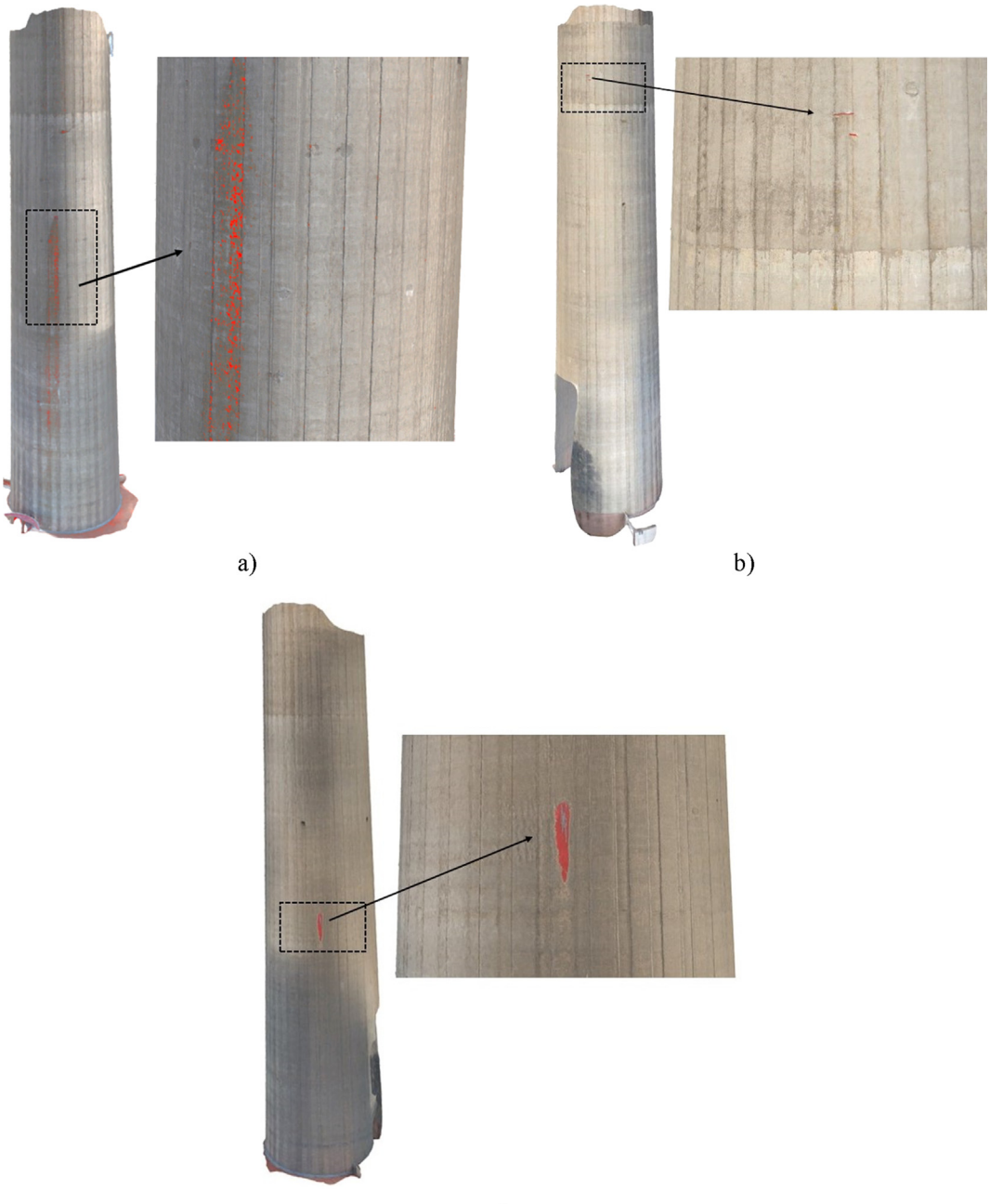

Fig. 13. 3D geometric model of the structure reconstituted in the Pix4Dmapper software, considering the overlap of: a) biological colonies, b) exposed steel rebars, c) efflorescences (all in false colors).

4.5. BIM integration

A 3D geometric model of the tower, including the material properties and the phasing of the construction process, was developed in the Autodesk Revit platform (Fig. 14). The geometric generation of the concrete shaft was performed with the aid of the graphical programming tool Dynamo, considering the limitations of Revit regarding the autonomous generation of the wall in the shape of a hyperboloid of revolution. The geometry and structural properties of the metallic tower were imported from an existing numerical model developed in the Autodesk Robot software [37]. The masks of the various identified pathologies were incorporated into the BIM model using the Autodesk Navisworks software. As an example, Fig. 14 depicts the biological colonies mask on the external layer of the tower shaft, between the 30 m and 60 m levels.

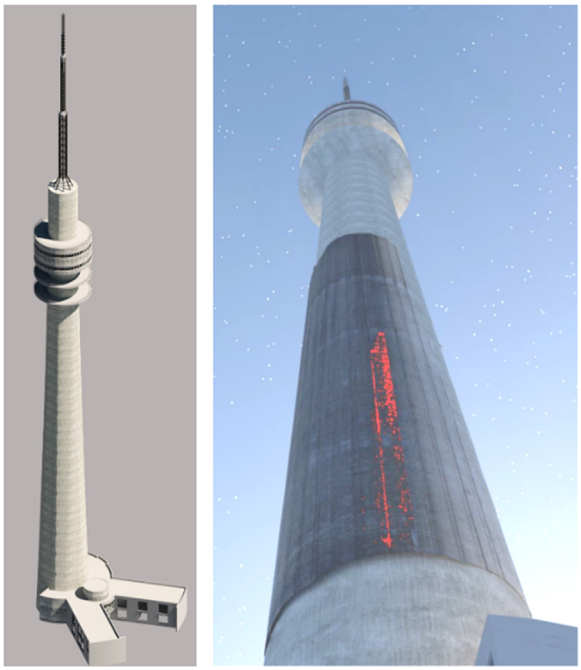

Fig. 14. BIM model of the tower with the biological colonies mask.

5. Conclusions

Contactless and remote structural surveys are of the utmost importance in general situations, and especially in structures with poor accessibility due to their geographical location, geometrical characteristics or other reasons, requiring dangerous and/or expensive interventions, often with special equipment and limited capability.

This work describes a methodology for the remote inspection of RC structures using UAVs with the integration of the results into BIM models based on advanced digital image processing techniques and the application of heuristic feature extraction methods developed in MATLAB©.

The use of this methodology in the remote inspection of the RC shaft of the Monte da Virgem telecommunications tower demonstrated robustness and efficiency in three of the studied pathologies (biological colonization, efflorescences and exposed steel rebars) and also showed the general absence of visible cracks in the structure.

The availability of the inspection results through the superposition of false color pathology maps in the BIM model also proved to be an efficient and self-explanatory way of making the results available to the infrastructure manager.

In future inspections, the proposed methodology will provide terms of comparison regarding the evolution of pathologies over time, allowing the study of their propagation and a timely calendarization of maintenance interventions.

Future works intend to develop sets of criteria for the automatic assessment of the evolution of pathologies by means of damage indicators adapted to the specific characteristics of each case. In addition to the damage features already stablished, new features (e.g., crack width, efflorescence thickness, etc.) will also be implemented to provide further information for decision making. The comparison between the results of the remote inspection methodology and the results from visual inspections will allow the appropriate validation of the proposed methodology. Other works under consideration will address the advantages of using multispectral cameras to record wavelengths beyond the visible spectrum, and the development of stronger algorithms based on the application of artificial intelligence for the automatic identification of cracks and exposed steel reinforcements (e.g. Convolutional Neural Networks).

Declaration of Competing Interest

The authors declared that there is no conflict of interest.

Acknowledgements

The authors would like to thank Altice, in particular Eng. Jorge Garcia, for supporting the inspection campaigns in the Monte da Virgem telecommunications tower, HP Drones, in particular Mr. Hanniel Pontes, for the loan of equipment to carry out the campaigns, and to Eng. Rafael Cabral and Eng. Gabriel Saramago, for their support in operating the UAV and preparing the inspection campaigns. The authors acknowledge the Base Funding - UIDB/04708/2020 of the CONSTRUCT - Instituto de I&D em Estruturas e

Construções - funded by national funds through the FCT/MCTES (PIDDAC).

References

[1] F. Stochino, M. Fadda, F. Mistretta, Low cost condition assessment method for existing RC bridges, Eng. Fail. Anal. 86 (2018) 56–71.
[2] A. Orcesi, D. Frangopol, S. Kim, Optimization of bridge maintenance strategies based on multiple limit states and monitoring, Eng. Struct. 32 (3) (2010) 627–640.
[3] B. Spencer, V. Hoskere, Y. Narazaki, Advances in computer vision-based Civil infrastructure inspection and monitoring, Engineering. 5 (2019) 199–222.
[4] Y.-J. Cha, W. Choi, O. Buyukozturk, Deep learning-based crack damage detection using convolutional neural networks, Comput.-Aided Civ. Infrastruct. Eng. 32 (5) (2017) 361–378.
[5] T. Hutchinson, Z. Chen, Improved image analysis for evaluating concrete damage, J. Comput. Civil Eng. 20 (3) (2006) 210–216.
[6] M. Vázquez, E. Galán, M. Guerrero, P. Ortiz, Digital image processing of weathered stone caused by efflorescences: a tool for mapping and evaluation of stone decay, Constr. Build. Mater. 25 (4) (2011) 1603–1611.
[7] C. Dung, H. Sekiya, S. Hirano, T. Okatani, C. Miki, A vision-based method for crack detection in gusset plate welded joints of steel bridges using deep convolutional neural networks, Autom. Constr. 102 (2019) 217–229.
[8] H.-K. Shen, P.-H. Chen, L.-M. Chang, Automated steel bridge coating rust defect recognition method based on color and texture feature, Autom. Constr. 31 (2013) 338–356.
[9] T. Barkavi, C. Natarajan, Processing digital image for measurement of crack dimensions in concrete, Civil Engineering Infrastructures J. 52 (1) (2019) 2093–2322.
[10] S. Sankarasrinivasan, E. Balasubramanian, K. Karthik, U. Chandrasekar, R. Gupta, Health monitoring of civil structures with integrated UAV and image processing system, Procedia Comput. Sci. 54 (2015) 508–515.
[11] Y. Xu, Y. Bao, J. Chen, W. Zuo, H. Li, Surface fatigue crack identification in steel box girder of bridges by a deep fusion convolutional neural network based on consumer-grade camera images, Struct. Health Monitoring. 18 (3) (2019) 653–674.
[12] X.-W. Ye, T. Jin, C.-B. Yun, A review on deep learning based structural health monitoring of civil infrastructures, Smart Structures Systems. 24 (5) (2019) 567–586.
[13] N.-D. Hoang, Q.-L. Nguyen, Metaheuristic optimized edge detection for recognition of concrete wall cracks: a comparative study on the performances of Roberts, Prewitt, Canny, and Sobel algorithms, Adv. Civil Eng. 7163580 (2018).
[14] G. Bayar, T. Bilir, A novel study for the estimation of crack propagation in concrete using machine learning algorithms, Constr. Build. Mater. 215 (2019) 670–685.
[15] I. Abdel-Qader, O. Abudayyeh, M. Kelly, Analysis of edge-detection techniques for crack identification in bridges, J. Comput. Civil Eng. 17 (4) (2003) 255–263.
[16] S. Li, X. Zhao, Image-based concrete crack detection using convolutional neural network and exhaustive search technique, Adv. Civil Eng. 6520620 (2019).
[17] B. Wang, W. Zhao, P. Gao, Y. Zhang, Z. Wang, Crack damage detection method via multiple visual features and efficient multi-task learning model, Sensors. 18 (2018) 1796.
[18] H. Kim, E. Ahn, M. Shin, S.-H. Sim, Crack and noncrack classification from concrete surface images using machine learning, Struct. Health Monitoring. 18 (3) (2019) 725–738.
[19] H.-G. Moon, J.-H. Kim, Intelligent crack detecting algorithm on the concrete crack image using neural network, Proceedings of 28th International Symposium on Automation and Robotics in Construction, 2011,, pp. 1461–1467.
[20] H. Kim, J. Lee, E. Ahn, S. Cho, M. Shin, S.-H. Sim, Concrete crack identification using a UAV incorporating hybrid image processing, Sensors. 17 (2017) 2052.
[21] T. Nishikawa, J. Yoshida, T. Sugiyama, Y. Fujino, Concrete crack detection by multiple sequential image filtering, Comput.-Aided Civ. Infrastruct. Eng. 27 (1) (2012) 29–47.
[22] A. Mohan, S. Poobal, Crack detection using image processing: a critical review and analysis, Alexandria Engineering J. 57 (2018) 787–798.
[23] P. Oyekola, A. Mohamed, J. Pumwa, Robotic model for unmanned crack and corrosion inspection, Int. J. Innovative Technology and Exploring Engineering. 9 (1) (2019) 862–867.
[24] B. Kim, S. Cho, Automated vision-based detection of cracks on concrete surfaces using a deep learning technique, Sensors. 18 (2018) 3452.
[25] R. Nigam, S. Singh, Crack detection in a beam using wavelet transform and photographic measurements, Structures. 25 (2020) 436–447.
[26] W. Silva, D. Lucena, Concrete cracks detection based on deep learning image classification, Proceedings. 2 (2018) 489.
[27] Y.-K. An, K.-Y. Yang, B. Kim, S. Cho, Deep learning-based concrete crack detection using hybrid images, Proc. SPIE Sensors and Smart Structures Technologies for Civil, Mechanical, and Aerospace Systems. 1059812 (2018).
[28] D. Ciresan, U. Meier, J. Masci, L. Gambardella, J. Schmidhuber, Flexible, high performance convolutional neural networks for image classification, Proceedings of the Twenty-Second International Joint Conference on Artificial Intelligence, 2011, pp. 1237–1242.
[29] T. Rakha, A. Gorodestsky, Review of Unmanned Aerial System (UAS) applications in the built environment: towards automated building inspection procedures using drones, Autom. Constr. 93 (2018) 252–264.
[30] H. Kim, E. Ahn, S. Cho, M. Shin, S.-H. Sim, Comparative analysis of image binarization methods for crack identification in concrete structures, Cem. Concr. Res. 99 (2017) 53–61.
[31] I.-H. Kim, H. Jeon, S.-C. Baek, W.-H. Hong, H.-J. Jung, Application of crack identification techniques for an aging concrete bridge inspection using an unmanned aerial vehicle, Sensors. 18 (6) (2018) 1881.
[32] T. Omar, M. Nehdi, Remote sensing of concrete bridge decks using unmanned aerial vehicle infrared thermography, Autom. Constr. 83 (2017) 360–371.
[33] S. Dorafshan, R. Thomas, M. Maguire, Fatigue crack detection using unmanned aerial systems in fracture critical inspection of steel bridges, J. Bridge Eng. 23 (10) (2018) 04018078.
[34] MathWorks (2018). Image Processing Toolbox: User's Guide (R2018b). Natick, Massachusetts, USA.
[35] F. Bandini, D. Olesen, J. Jakobsen, C. Kittel, S. Wang, M. Garcia, P. Bauer-Gottwein, Technical note: Bathymetry observations of inland water bodies using a tethered single-beam sonar controlled by an unmanned aerial vehicle, Hydrol. Earth Syst. Sci. 22 (2018) 4165–4181.
[36] D. Ribeiro, J. Leite, N. Pinto, R. Calçada, Continuous monitoring of the dynamic behaviour of a high-rise telecommunications tower, Structural Design of Tall and Special Buildings. 28 (11) (2019) e1621.
[37] Ribeiro D, Leite J, Pauli R, Alves V, Costa B, Calçada R. Calibration of the numerical model of a telecommunications tower based on genetic algorithms. Chapter 3. Genetic Algorithms: Advances in Research and Applications. 2017. Nova Publishers, USA. ISBN 978-1-53611-856-8.